scientific reports

Check for updates

OPEN

Mitochondrial aldehyde dehydrogenase restores the migratory capacity inhibited by high glucose-induced hyperosmolality

Chi-Cheng Huang[1,2], Yuh-Lien Chen[2] & Chung-Liang Chien[2]✉

Cell migration, which is often impaired under high glucose (HG) conditions, plays a crucial role in the pathogenesis of various diabetic complications. This study investigates the role of mitochondrial aldehyde dehydrogenase (ALDH2) in the HG-induced migratory inhibition. Using fibroblasts sub-cultured in HG medium as a cell model of chronic hyperglycemia, we found that prolonged exposure to HG stress inhibited cell migration via a novel mechanism independent of oxidative stress or cell death. By increasing osmolality, HG induced perinuclear clustering of mitochondria, enhanced focal adhesion maturation, and caused the cells to be less responsive to migratory cues. The pharmacological inhibition of ALDH2 exaggerated this phenomenon, while ALDH2 overexpression protected cells from the migratory impairment caused by HG-induced hyperosmolality. Cells with ALDH2 overexpression exhibited less mature focal adhesions and longer mitochondrial network, suggesting that ALDH2 might preserve mitochondrial integrity to facilitate the focal adhesion turnover during cell migration.

Keywords Cell migration, Hyperglycemia, Hyperosmolality, Focal adhesion, Cytoskeleton, Mitochondria, Aldehyde dehydrogenase

Cell migration is a complex and tightly regulated process essential for various physiological phenomena including angiogenesis and tissue repair[1,2]. The cytoskeleton, comprised of actin filaments, microtubules, and intermediate filaments, plays a central role in orchestrating cell migration[3,4]. It interacts with other cells and the extracellular matrix through cell adhesion molecules like paxillin to determine cell polarity[5,6]. The dynamic assembly and disassembly of focal adhesions is crucial for cell migration by driving cell protrusions and rear retraction[7]. High glucose (HG), particularly in the context of diabetes mellitus, may disrupt cytoskeleton remodeling and impede cell migration[8,9].

Delayed wound healing and increased susceptibility to wound infections are common in individuals with diabetes due to the impaired migratory capacity of neutrophils, fibroblasts, and endothelium under hyperglycemic stress[9,10]. HG has been shown to cause destabilization of lamellipodia through a mechanism that impairs cell polarity and adhesion maturation[9]. Other researchers found that adhesion strength was significantly increased in endothelium cultured on glycated collagen-coated surfaces due to a switch of integrin subtypes[10]. However, the underlying mechanisms by which HG affects intracellular cytoskeleton remodeling and focal adhesion turnover remains poorly understood, and clarifying these mechanisms holds tremendous potential for developing interventions to improve the outcomes of diabetic patients[11].

Aldehyde dehydrogenase (ALDH) is a gene superfamily of phase I oxidizing enzymes that is responsible for the detoxification of both exogenous and endogenous aldehydes, and cytosolic ALDH1A1 and mitochondrial ALDH2 are the two major isozymes found in human tissues[12]. ALDH2 is best known for its role in alcohol metabolism and its association with the "Asian flush syndrome"[13]. A loss-of-function point mutation (ALDH2*2, Glu504Lys), which reduces the enzymatic activity by 60–80% in heterozygotes, causes rapid accumulation of acetaldehyde and facial flushing after drinking alcohol[14]. Furthermore, emerging evidence based on ALDH2*2

[1]Division of Cardiology, Cardiovascular Medical Center, Far Eastern Memorial Hospital, New Taipei City, Taiwan. [2]Graduate Institute of Anatomy and Cell Biology, College of Medicine, National Taiwan University, Taipei, Taiwan. ✉email: chien@ntu.edu.tw

knock-in/knock-out mouse model or human health records suggested that ALDH2 deficiency may be linked to increased susceptibility to diet-induced obesity, glucose intolerance, and other metabolic disorders[15,16].

In this study, we aimed to investigate the role of ALDH2 in the HG-induced inhibition of cell migration. Although we utilized the ALDH2 inhibitor disulfiram to simulate cells with ALDH2 deficiency, the primary results centered on 3T3 fibroblasts with ALDH2 overexpression achieved via lentiviral-based plasmids. Cells with different ALDH2 activities were sub-cultured in hyperglycemic/ hyperosmolar medium for 2–7 days. Wound healing assay, flow cytometry, immunofluorescent staining, and Western blot were performed to investigate how ALDH2 modulates the HG-induced inhibition of cell migration through mechanisms associated with the cytoskeleton and focal adhesions.

Material and methods

Cell culture and treatment protocols

NIH/3T3 mouse fibroblasts (ATCC CRL-1658) were maintained in Dulbecco's Modified Eagle's Medium (DMEM) (Gibco, NY, USA) supplemented with 10% fetal bovine serum (Gibco, cat #2286113RP) and 1% penicillin–streptomycin (Biological Industries, Israel). The culture media contained 25 mM D-glucose (Ctrl), 55 mM D-glucose (high glucose, HG), or 25 mM D-glucose + 30 mM D-mannitol (osmotic control, OC) according to the protocols. The ALDH2 inhibitor disulfiram (Merck, cat #86720) was added to various media at a concentration of 1–6 μM to decrease the enzymatic activity of 3T3 fibroblasts. Unless otherwise specified, cells were plated at a density of 3×10^5 cells/10 cm dish (Corning, NY, USA) and cultured at 37 °C, 95% air, 5% CO2, and 100% humidity; passage was performed every 3 days.

Fluorescent-conjugated bicistronic plasmids

The construction of plasmid pEGFP-ALDH2 and stable clones was performed initially using the protocol described in our previous study[17]; however, all transfected cells died within 48 h, likely due to aggregation of misfolded EGFP-ALDH2 fusion protein in mitochondria (Suppl. Figure 1a). We therefore designed the bicistronic pEGFP-T2A-ALDH2 plasmid, which translates the enhanced green fluorescent protein (EGFP) and ALDH2 separately (Fig. 1a–c). We cloned the ALDH2 sequence from the pcDNA3.1-ALDH2 plasmid (a gift from Dr. Che-Hong Chen at Stanford University) and added the *EcoR1* cutting site plus T2A sequence at the 5' end. The PCR primers specifically designed were: 5′-ATCGGAATTCCGAAGGACGAGGATCACTAC TAACATGTG-3′ and 3′-GGATCCTCTAGAACTTTCTTGACCCAAGAGATTTTGTA-5′. The T2A-ALDH2 PCR product was inserted into the pEGFP-C1 vector cut by *EcoRI* and *BamHI*, and the plasmid was amplified according to the manufacturer's protocol. The plasmids were sent for DNA sequencing (Genomics, Taiwan) before proceeding for transfection.

Electroporation and selection of stable clones

The 3T3 fibroblasts were trypsinized, washed with phosphate-buffered saline (PBS), and resuspended in serum-free DMEM before being gently mixed with plasmid DNA (1.5×10^6 cells + 3 μg of DNA) on ice. After transferring to a 4 mm cuvette (BTX, MA, USA), a 300 mV electric pulse was applied using an ECM 2001 system (BTX) for 20 ms. The cells were immediately mixed with warm complete growth medium and plated into a 3.5 cm cell culture dish. The medium was changed to fresh growth medium the following morning, and cells were cultured for another 48–72 h until confluence. The selection process was then started using Geneticin (Gibco, cat #11,811,031) as described previously[17]. In brief, DMEM containing Geneticin 800 μg/ml killed almost all non-transfected cells within 5–7 days; the remaining colonies were trypsinized and re-plated in fresh growth medium, of which cell growth recovered after 7–10 days. The stable clones were then maintained in various media containing Geneticin 400 μg/ml, and the expression of ALDH2 was checked regularly by the presence of green fluorescence. The stable clones were re-labeled as passage N + 1, and cells less than passage N + 20 were used for experiments.

ALDH2 activity assay

To specify the exact ALDH2 activity in different treatment groups, we developed a 96-well-based activity assay modified from methods described in a previous study[18]. The 3T3 fibroblasts were plated at a density of 3×10^5 per 6 cm dish and grew overnight, followed by changing the medium to Ctrl/OC/HG for an incubation of 48 h; when ALDH2 inhibition was needed, disulfiram was added at the time of changing media with a final concentration of 6 μM. The cells were scraped off and incubated on ice for 20 min with 200 μl extraction buffer containing CelLytic MT and 1% protease/phosphatase inhibitor (Sigma-Aldrich, MO, USA). The cell lysates were then centrifuged at 16,000 g for 5 min at 4 °C, and the supernatants were collected. The supernatants of whole cell lysate were mixed in a 1:4 ratio with working solution containing 100 mM sodium pyrophosphate (pH 9.0), 10 mM NAD+, and 10 mM propionaldehyde (all in final concentration) to start the enzymatic reaction. The final reaction solution was transferred into a 96-well Clear-Bottom Polystyrene High-Bind Microplate (Corning, cat. #9018) and examined by a microplate reader (Ultrospec® 3100 pro; Amersham Bioscience Corp., Piscataway, NJ) using the kinetic mode. Because ALDH2 removes hydrogen from propionaldehyde to produce NADH, which has peak absorption at 340 nm, the OD_{340} over time was measured to represent enzymatic activity. As the reaction may occur spontaneously, the OD_{340} of blank samples was subtracted from each treatment group. ALDH2 activity was calculated as the average change in OD_{340} from 5 to 30 min, when the rate of NADH production was almost tangential and mainly limited by enzymatic activity. The OD_{340} of each reaction was normalized using values obtained from three replicated wells.

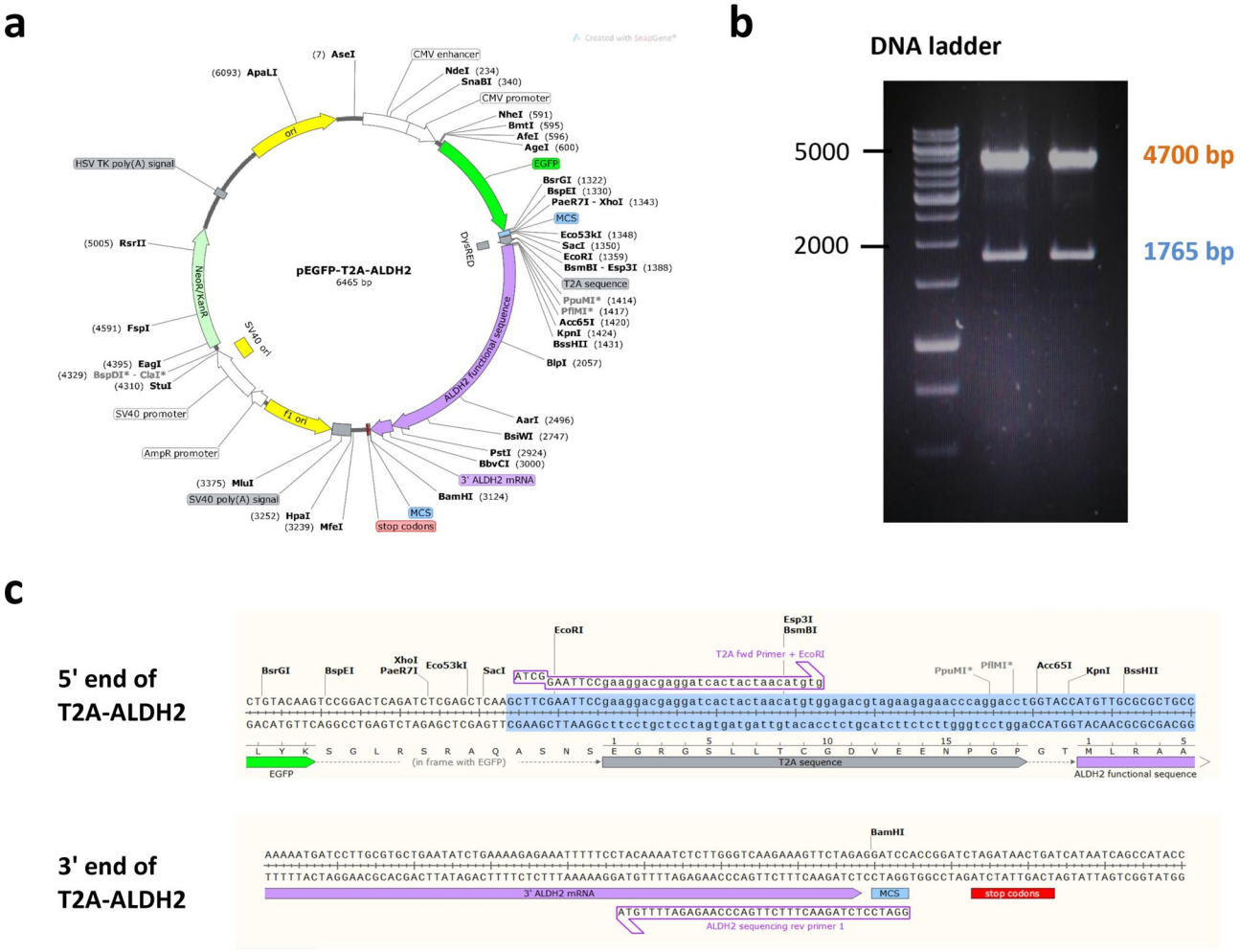

Fig. 1. The overexpression of mitochondrial aldehyde dehydrogenase (ALDH2) in NIH/3T3 fibroblasts using bicistronic plasmid. (**a**) The schematic map of bicistronic plasmid pEGFP-T2A-ALDH2, which concurrently expresses the enhanced green fluorescent protein (EGFP) and ALDH2. (**b**) The construction of pEGFP-T2A-ALDH2 involved the ligation of T2A-ALDH2 insert (1765 bp) into the pEGFP1-C1 vector (4700 bp) cut by restriction enzymes *EcoRI* and *BamHI*. Agarose gel electrophoresis was performed to purify the digested vector before it was retrieved for ligation, as well as to confirm the size of both the vector and insert after the completion of ligation. (**c**) During the cloning of ALDH2 sequence, the T2A sequence plus cutting site of *EcoRI* was added to the 5' end using a specifically designed primer. (**d**) The immunostaining of ALDH2 on 3T3-pT2A-ALDH2 stable clone was either spotty, elongated, or connected into branched networks, characteristic of normal mitochondria. Scale bars = 10 μm.

Flow cytometry

At the end of treatment in each group (incubation in Ctrl/OC/HG medium for 48 h; in Ctrl/OC/HG +/− disulfiram 6 μM for 4 h), we performed flow cytometry to determine cell death and oxidative stress. Both the trypsinized and detached cells in the medium were collected and incubated with CellROX Deep Red 500 nM (Invitrogen, cat. #C10422) at 37 °C for 30 min; this dye exhibits a strong fluorescence signal (644/665 nm) once oxidized by intracellular free radicals. The cells were then washed and incubated at 37 °C for 15 min with SYTOX Blue 1 μM (Invitrogen, cat. #S34857); this dye binds to the nucleic acid of dead cells through their compromised membranes and exhibits bright blue fluorescence (444/480 nm). After both incubation periods, the cells were transferred to 5 ml filter tubes (Falcon, REF352235) and analyzed immediately using an LSRFortessa™ Cell Analyzer (BD Life Science, NJ, USA). The excitation/emission spectrum of two reagents allowed for the simultaneous identification of reactive oxygen species (ROS) and cell death. Data were analyzed using FlowJo software (BD Life Science).

Wound healing assay

Before the wound healing assay, the 3T3 fibroblasts were sub-cultured in different media for 7 days, then seeded at a density of 2×10^5 cells per 24-well plate and grown to confluence overnight. A wound was created by scratching with a sterile pipette tip in the center of the plate, which was then washed with PBS. Progress of wound closure was photographed every 8 h using an inverted microscope in a time-lapse manner. At least three separate images were acquired at each time point, and the average area of the wound was measured using ImageJ (NIH, USA) and expressed as the percentage compared to 0 h.

Immunofluorescent staining

To identify intracellular structures, coverslips coated with 1% gelatin (Sigma-Aldrich) were placed in advance into the culture vessels. After completing individual treatment protocols, the cells were washed with PBS and incubated with serum-free DMEM containing Mitotracker Red CMXRos 100 nM and Hoechest 34,580 10 μg/ml for 30 min (Invitrogen) when mitochondrial/nuclear staining was needed. The cells were then fixed by 4% paraformaldehyde (Sigma-Aldrich) in PBS (pH 7.4) at 37 °C for 15 min, permeated with PBS-T, and blocked by 3% FBS at room temperature for 30 min. After removing the blocking buffer, the cells were incubated at 4 °C overnight with primary antibodies (1:200): anti-EGFP (Sigma-Aldrich, cat. #AB3080), anti-ALDH2 (Sigma-Aldrich, #ab115348), or anti-Paxillin (Cell Signaling, #2542). Fluorophore-conjugated secondary antibodies or Alexa Fluor 594 phalloidin (Invitrogen, A12381) were applied the next morning and allowed to incubate at room temperature for 1 h. The coverslips were washed three times with PBS-T between each step, mounted in Fluoro-Gel (Laborimpex, #17985-11), and stored in the dark before further microscopic examinations.

Mitochondrial morphology analysis

To analyze the mitochondrial morphology, the ImageJ plug-in "Mitochondrial Analyzer" was utilized according to developer's guidance[19]. It began with the pre-processing of 8-bit 2D images using the default settings (background subtraction: 1.25 micron; sigma filtering radius: 0.97; local contrast enhancement maximal slope: 1.80; gamma adjustment: 0.80). Adaptive thresholding was applied for a block size of 1.35 micron and C-value of 5; cut-off values were optimized to effectively distinguish individual mitochondria (by direct visual comparison between different sets of values). Post-thresholding steps included de-speckling and outlier removal, using a radius of 1.0 pixel, to ensure accurate representation of mitochondrial morphology. The analyzer's integrated tools were used for quantifying morphological parameters such as mitochondrial area, perimeter, form factor, and aspect ratio, as well as network features like branching and junction counts derived from skeletonization. These metrics enabled detailed assessment of mitochondrial structural complexity and connectivity. A minimum of three distinct images were taken from each treatment group (e.g., 3T3-C1 HG), and the parameters were computed as the average of these three images.

Western blot

After being sub-cultured in different media for 7 days, the fibroblasts were harvested, and total protein was extracted using CelLytic MT buffer supplemented with 1% protease/phosphatase inhibitor as described above. The protein concentration was determined using a Bradford assay, and 5 μg of protein was loaded onto a sodium dodecyl sulfate–polyacrylamide gel for electrophoresis (90–110 V). Separated proteins were then transferred onto a PVDF membrane. The membrane was subsequently blocked in 5% non-fat milk for 1 h, probed with primary antibodies (1:1000) targeting Paxillin, MFN2 (Proteintech, Cat No. 12186-1-AP), DRP1 (Cell Signaling, D9A1 #4494), and Mff (Cell Signaling, E5W4M #84,580) by incubation at 4 °C overnight, followed by appropriate horseradish peroxidase-conjugated secondary antibodies (1:2500) at room temperature for 1 h. Protein bands were visualized using enhanced chemiluminescent detection using a BioSpectrum Imaging System (UVP, CA, USA). The intensity of individual bands was quantified by ImageJ and normalized as compared to the intensity of GAPDH bands.

Statistical analysis and representative plots

We used Prism 9 software (GraphPad, MA, USA) for the generation of representative plots and statistical analysis. All values within figures were presented as mean +/− standard error of mean (SEM) as the error bars, and the number of repetitions was shown whenever available. Statistical significance was defined as $p < 0.05$ using the two-way ANOVA analysis.

Results

Transfection of the p-EGFP-T2A-ALDH2 bicistronic plasmid significantly increased the ALDH2 activity

The transfection efficiency of pEGFP-C1 and pEGFP-T2A-ALDH2 via electroporation was roughly 10% (Suppl. Figure 1b). After 7 days of selection using medium containing Genecitin 800 μg/ml, which killed > 90% of non-transfected cells, the presumably stable clones were re-plated in fresh growth medium. The second round of selection was repeated 2 weeks after the recovery of cell growth, and this time Geneticin only slowed cell growth without causing cell death (Suppl. Figure 1c). Both the 3T3-pEGFP-C1 and 3T3-pT2A-ALDH2 stable clones displayed weak cytosolic green fluorescence that could be identified by immunofluorescent staining (Fig. 1d). The mitochondrial staining of ALDH2 co-localized with Mitotracker and was characterized as small fine dots that were either elongated, branched, or connected into networks (Suppl. Figure 1d). Because the 3T3 fibroblasts do have an endogenous expression of ALDH2, we performed the activity assays to confirm the success of ALDH2 overexpression. It was revealed that the ALDH2 activity of 3T3-pT2A-ALDH2 was significantly higher than that of 3T3-pEGFP-C1 (Fig. 2a). The difference in enzymatic activity between the two clones, namely the level increased by plasmid-mediated ALDH2 overexpression, was consistent in all treatment groups (Fig. 2c).

Inhibition of ALDH2 by disulfiram increased oxidative stress and cell death; it also appeared to prohibit cell migration and proliferation

Due to a high basal expression of ALDH2 in the 3T3-pEGFP-C1 clones, we used disulfiram to test how ALDH2 inhibition might affect fibroblast cell behavior. We found that disulfiram significantly inhibited ALDH2 activity (Fig. 2b,c). The cell density was lower in cells cultured in media containing disulfiram 6 μM for 24 h compared to those in the control groups, and many cells were almost detached from the culture plates (Suppl. Figure 2a). Membrane blebbing morphology suggested an increase in cell death, and this was subsequently confirmed by flow cytometry analysis of cells incubated in various media with disulfiram for 4 h, which showed that most of the detached cells had died due to oxidative stress (Suppl. Figure 2b). The cytotoxic effect of disulfiram appeared to be affected by cell density and drug concentration, so when we decreased the disulfiram concentration to 2 μM, the 3T3-pEGFP-C1 clones survived but grew slowly to form large colonies (Suppl. Figure 2c). The cell density was much higher in the center than the periphery of colonies, and the size of colonies was constantly smaller in the HG + D group compared to the Ctrl + D group. These findings implied that both cell proliferation and migration were impaired in fibroblasts with ALDH2 inhibition, and that these impairments could be aggravated by HG stress.

High glucose/osmolality significantly inhibited cell migration, and the inhibitory effect became less evident in cells with ALDH2 overexpression

To clarify how HG affects cell behavior and to avoid the variable inhibitory effects of disulfiram depending on cell density, we used the 3T3-pEGFP-C1 and 3T3-pT2A-ALDH2 stable clones for the latter experiments. Flow cytometry was performed using fibroblasts exposed to the Ctrl/HG/OC medium for 48 h, and the results revealed no difference in cell death or production of ROS (Fig. 3a). We sub-cultured these stable clones in different media for 7 days, but no change in cell morphology or doubling time was noted. However, the wound healing assay showed that cell migration was significantly impaired after sub-cultured in the HG or OC medium (Fig. 3b–e). The residual gap area was more than 40% in the 3T3-C1 HG/OC subclones 24 h after wound creation, and this was significantly larger than the 3T3-C1 Ctrl subclone, in which the gap healed almost completely (Fig. 3b,d). On the other hand, the residual gap area was about 25% in the 3T3-T2A HG/OC subclones, and the difference in cell migration was not statistically significant when compared with the 3T3-T2A Ctrl subclone (Fig. 3c,e). These findings demonstrated that prolonged exposure of the 3T3 fibroblasts to the HG/OC medium impaired their cell migration, and ALDH2 overexpression helps cells to be more resistant to this migratory inhibition effect.

High glucose/osmolality induced stress fiber reorganization and focal adhesion maturation, whose turnover was hindered during cell migration

To investigate the mechanisms of how HG/OC stress impaired cell migration, we examined the remodeling of stress fibers and focal adhesions under migration-promoting conditions. Cells were subcloned in the Ctrl/OC/HG medium for 7 days prior to wound healing assay and subsequently stained for F-actin and paxillin about 16–24 h after wounding. At the leading edge of artificial wound, the thin stress fibers often run along the longitudinal axis of the cell, parallel to direction of migration, forming lamellipodia that project forward in response to migration cues. Meanwhile, cells positioned further from the wound retained thick ventral stress fibers extending toward the periphery, suggesting their role in structural stability for non-migrating cells. (Fig. 4a–d). Compared to the 3T3-C1 Ctrl, the thick actin filaments were more abundant in the 3T3-C1 HG/OC subclones; similar trends were observed in the 3T3-T2A Ctrl vs. HG/OC subclones, but they were less prominent (Suppl. Figure 3a). These disoriented stress fibers tended to reorganize toward the trailing edge, ran in varying angles and directions irrelevant to the direction of cell migration, sometimes even outlined the cell border as seen in the 3T3-C1 HG subclone (Fig. 4f'). Conversely, most of the stress fibers ran parallel to the direction of cell migration in the 3T3-C1 Ctrl (Fig. 4e') and 3T3-T2A Ctrl/HG subclones (Fig. 4g', h').

We then focused on paxillin, a protein within focal adhesions that link integrin to actin cytoskeleton. Paxillin staining of nascent focal adhesions showed mostly fine speckles connected to elongated actin fibers, like those seen in the leading edge of the 3T3-C1 Ctrl subclone (Fig. 4e''), indicating these focal adhesions could rapidly dissemble preceding migratory readiness. On the contrary, paxillin staining of the 3T3-C1 HG subclone was often dense and larger in size (Fig. 4f''), a sign of mature focal adhesion exhibiting strong adhesion strength. The paxillin staining of the 3T3-T2A HG subclone was generally indifferent from that of the 3T3-T2A Ctrl subclone, both revealing punctate pattern in the lamellipodia (Fig. 4g'',h''). There was an obvious increase in

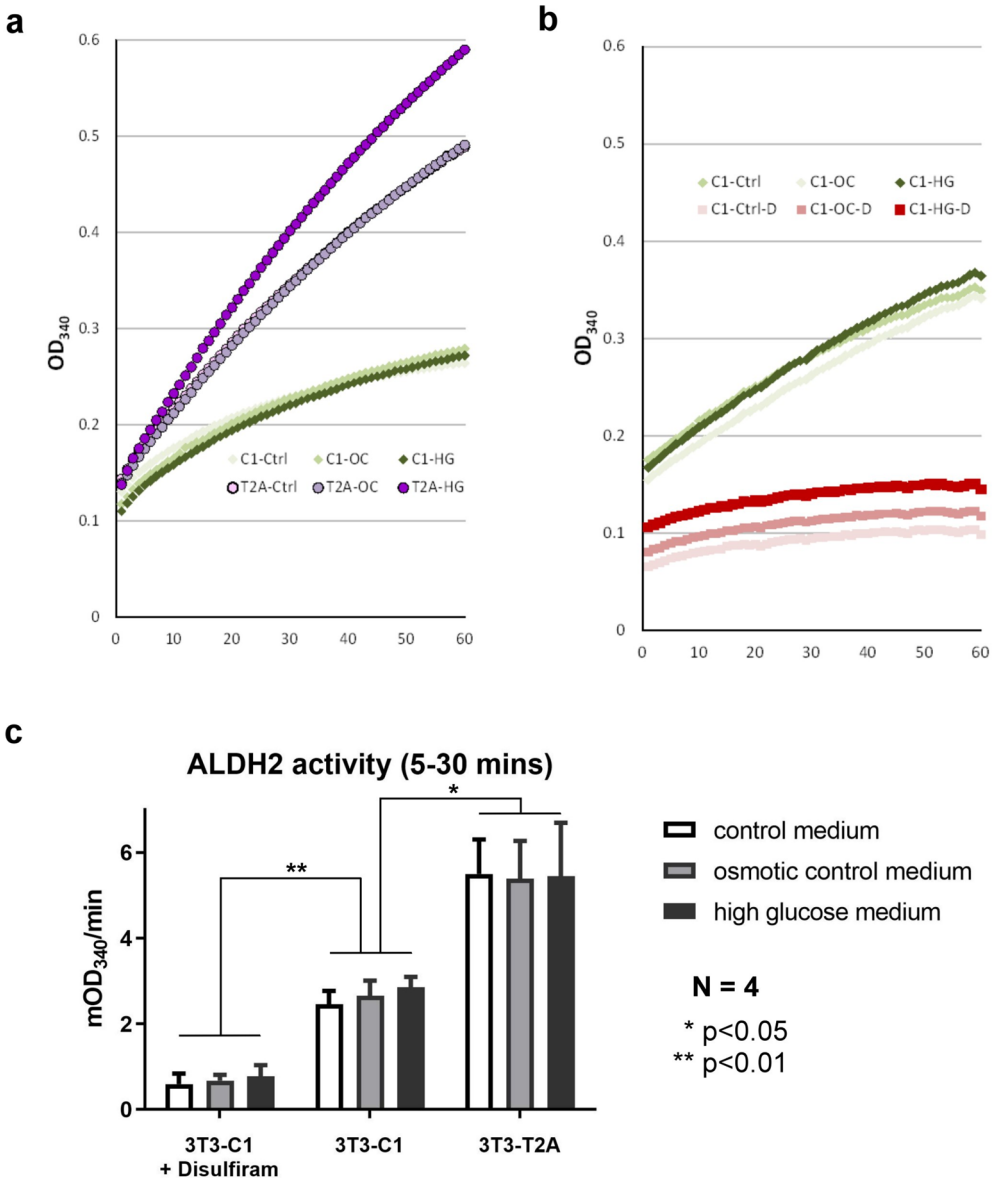

Fig. 2. The ALDH2 enzymatic activity of 3T3 in different treatment groups. (**a**) The OD_{340} measurements of 3T3-pEGFP-C1 (colored in green) and 3T3-pT2A-ALDH2 (colored in purple) cultured in the control (Ctrl), osmotic control (OC), and high glucose (HG) medium. (**b**) The results of 3T3-pEGFP-C1 cultured in the medium containing disulfiram 6 μM (Ctrl + D, OC + D, HG + D) were colored in red. Groups cultured in Ctrl/OC/HG medium without disulfiram were colored in green. (**c**) The ALDH2 activity of 3T3-pT2A-ALDH2 subclones were about 2 times higher than that of the 3T3-pEGFP-C1 subclones; meanwhile, disulfiram decreased the activity more than 50% irrespective of culture media. The ALDH2 activity assay was repeated 4 times between 3T3-C1 vs. 3T3-T2A and 3T3-C1 vs. 3T3-C1 + D groups. $^{*}p < 0.05$, $^{**}p < 0.01$.

mature focal adhesions in the 3T3-C1 HG/OC subclone, but not in the 3T3-T2A HG/OC subclones (Suppl. Figure 3b). When dense staining of paxillin was observed in the 3T3-T2A HG/OC subclones, it was less frequent in the protruding lamellipodia. Instead, it often appeared elongated and had good alignment with the stress fibers (Suppl. Figure 3c), highlighting active focal adhesions involved in mechano-transduction. Finally, western blot confirmed this up-regulation of paxillin in the 3T3-C1 HG/OC subclones, and the expression of paxillin notably decreased in all 3T3-T2A subclones (Fig. 4i,j). Taken together, our findings revealed that after prolonged exposure to HG-induced hyperosmolar stress, the 3T3 fibroblasts became more strongly adhered to the surface of culture vessels. ALDH2 facilitated focal adhesions turnover and enabled the cells to migrate efficiently toward the spatial and chemotactic signals created by artificial wounding.

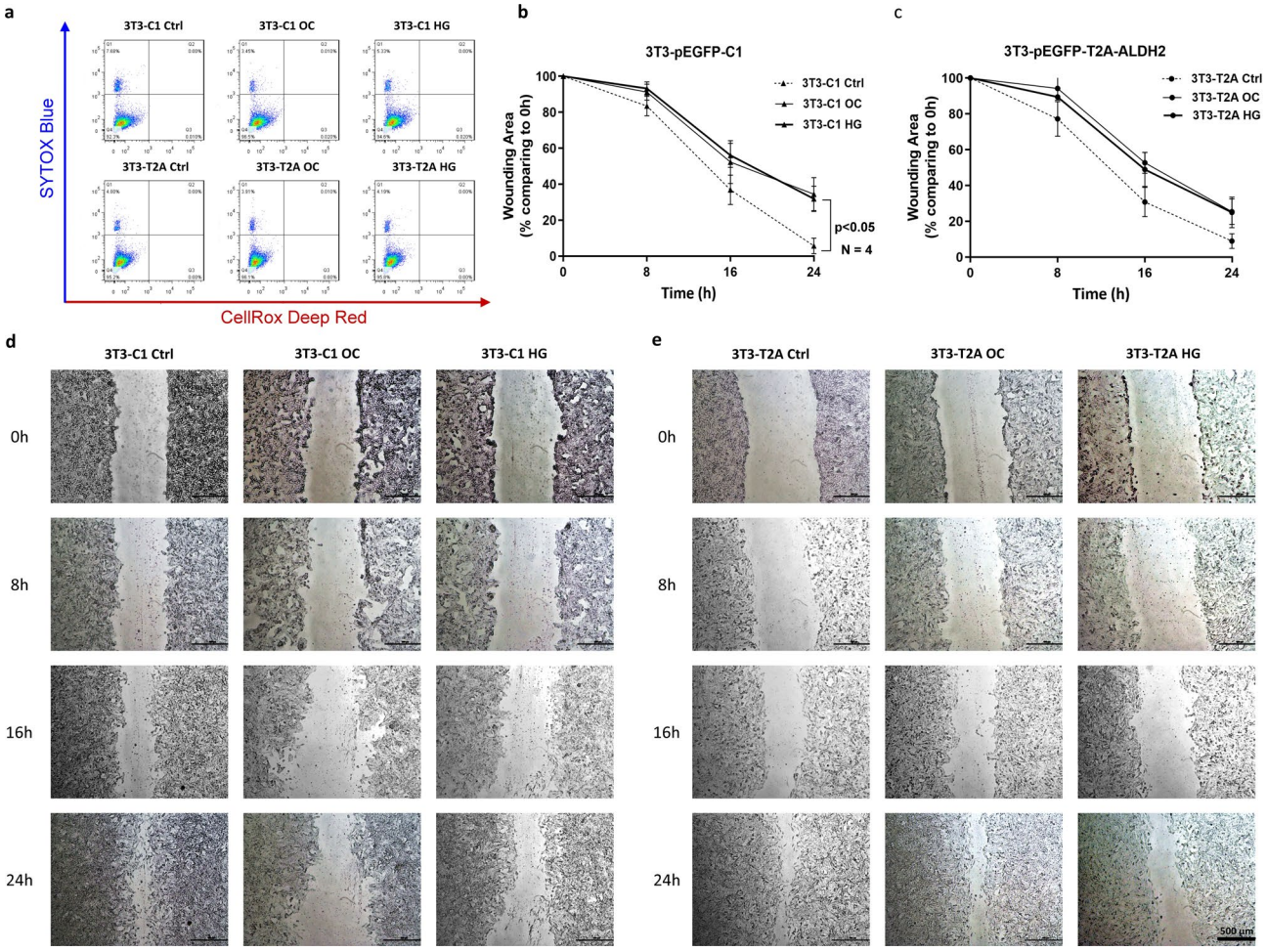

Fig. 3. Effects of ALDH2 overexpression on cell viability, oxidative stress, and migration ability in different NIH/3T3 subclones. (**a**) Flow cytometry revealed that sub-culture of 3T3-pEGFP-C1 and 3T3-pT2A-ALDH2 fibroblasts in the Ctrl/ OC/ HG medium did not lead to any change in cell death or oxidative stress. (**b**), (**d**) Wound healing assay of the 3T3-C1 subclones. In the 3T3-C1 Ctrl subclone, cell migration began between 8 and 16 h after wound creation and healed almost completely within 24 h. On the contrary, in the 3T3-C1 HG/ OC subclones, the mean residual gap area 24 h post-wounding was significantly larger (about 40%) than that of the 3T3-C1 Ctrl subclone. (**c**), (**e**) Wound healing assay of the 3T3-T2A subclones. In the 3T3-T2A HG/ OC subclones, the mean residual gap area 24 h after wound creation was roughly 25%, and it did not reach statistical significance when compared to the 3T3-T2A Ctrl subclone. Wound healing assay was repeated 4 times. Statistical significance was defined as $p < 0.05$. Each column represents different subclones; time-lapse images taken every 8 h are displayed in a row-wise order. Scale bars = 500 μm.

The turnover of focal adhesions was facilitated by the elongation of mitochondria, which could be restored by ALDH2 overexpression

To explore how ALDH2 affects focal adhesion turnover, paxillin and mitochondria were stained on cells subjected to the wound healing assay as described above to reveal the spatial relationships between mitochondria and cytoskeletons. We found that in the 3T3-C1 Ctrl and 3T3-T2A Ctrl subclones, mitochondria often fused into networks extending from the nucleus to cell periphery, especially to the protruding lamellipodia (arrow in Fig. 5a,c). In contrast, the mitochondria of non-migrating cells in the 3T3-C1 HG subclone were often condensed and clustered around nuclei (asterisk in Fig. 5b). Their paxillin was often strongly stained and located at the cell periphery, away from the mitochondrial networks (Fig. 5b',b''). Such a perinuclear clustering pattern of mitochondria was present in some cells in the 3T3-T2A HG subclone (asterisk in Fig. 5d), but cells with an elongated mitochondrial network were also noted (arrow in Fig. 5d).

To quantify the morphological changes of mitochondria after different treatments, Mitochondrial Analyzer was applied as described in the methods. One skeletonized mitochondrial network derived from the 3T3-C1 Ctrl subclone served as an example (Fig. 5e). Mitochondria in the protruding lamellipodia typically exhibit greater aspect ratio, form factor, area, and branch length. Meanwhile, those mitochondria clustered perinuclearly frequently appeared punctuated after skeletonization, displaying reduced area and branch length. The mean area and branch length per mitochondria were significantly lower in the 3T3-C1 HG/OC as compared to the 3T3-T2A HG/OC subclones (Fig. 5f–i), indicating that ALDH2 overexpression protected against the mitochondrial

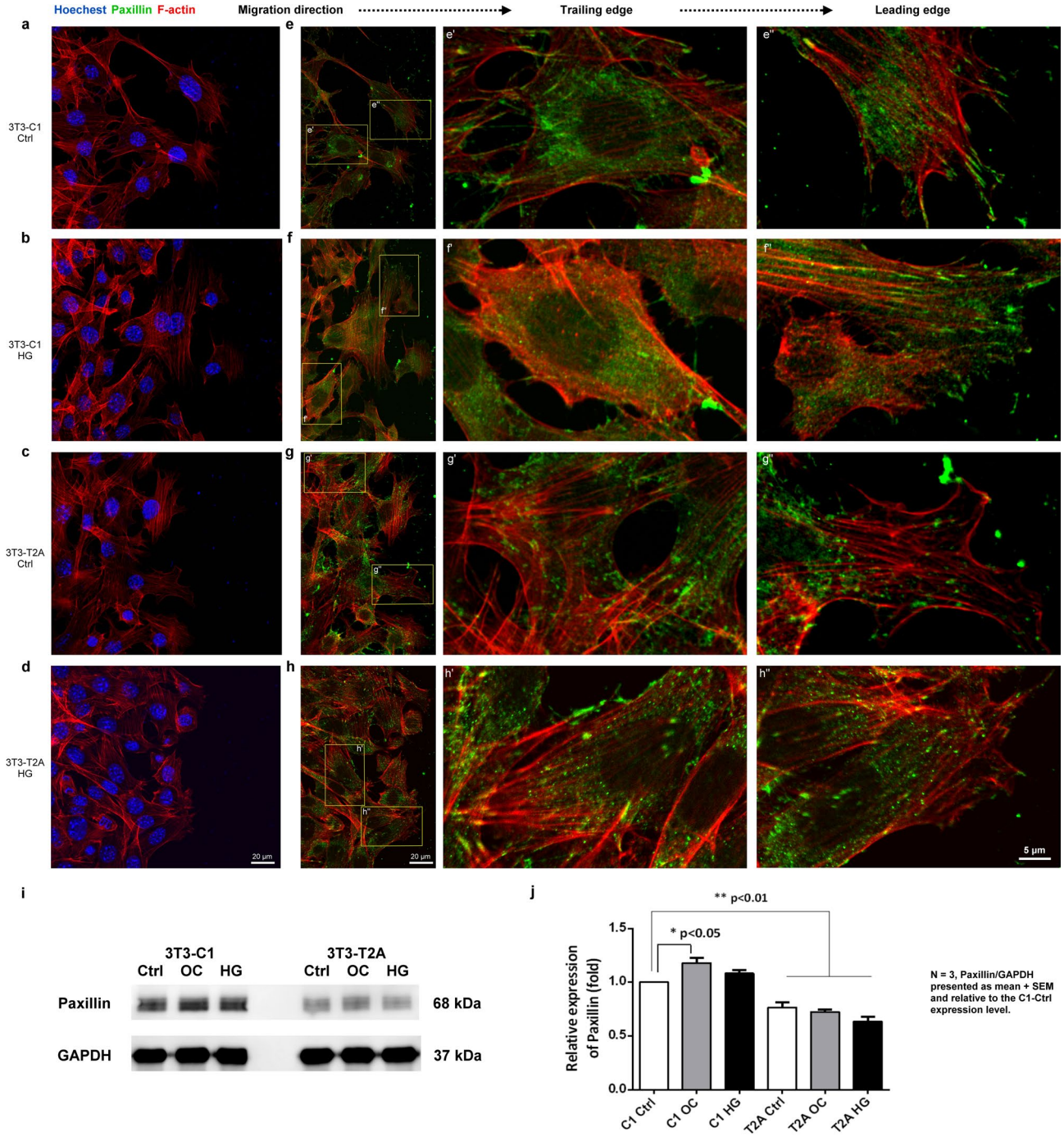

Fig. 4. Chronic HG/OC stress induced the focal adhesions maturation and stress fibers reorganization, which was mitigated by ALDH2. Confocal images of 3T3 fibroblasts under migration-promoting conditions are shown. Each row represents different subclones; all the wounds are placed on the right side. The right two columns are zoomed-in images from the second column, showing the trailing and leading edges, respectively. Scale bars = 20 μm (left two columns) or 5 μm (right 2 columns). When we combined only the labeling of (**a**–**d**) Hoechst plus F-actin, there was a significant reorganization of thick, disoriented actin filaments toward the trailing edge in the 3T3-C1 HG subclone. This phenomenon was less evident in the 3T3-T2A HG subclone, of which the organization of stress fibers was similar to that of 3T3-C1 Ctrl and 3T3-T2A Ctrl subclones. Examination on the relationship between (**e**–**f**) F-actin and Paxillin revealed fine speckles of paxillin linked to thin stress fibers in the 3T3-C1 Ctrl subclone, whereas in the 3T3-C1 HG subclones, densely-stained paxillin granules connected to thicker actin filaments. The paxillin staining pattern in the 3T3-T2A HG was indifferent from that of the 3T3-T2A Ctrl subclone, both displaying speckles or punctuates connected with stress fibers going parallel to the direction of cell migration. (**i**–**j**) Western blot showed that the expression of paxillin was up-regulated in the 3T3-C1 HG/OC subclones, but down-regulated in all the 3T3-pT2A-ALDH2 subclones. The Western blot was repeated 3 times; $^{*}P < 0.05$, $^{**}P < 0.01$

fragmentation induced by HG/OC stress. Surprisingly, there was no significant difference between subclones regarding the protein expressions of MFN2, DRP1, and Mff (Suppl. Figure 4). These findings suggest that mitochondrial networks may change their shape to support the disassembly of focal adhesions. This process could be inhibited by chronic exposure to HG/OC stress through mechanisms that are not related to ROS production or mitochondrial fission/fusion dynamics. The overexpression of mitochondrial ALDH2 restored mitochondrial elongation ability, reduced paxillin expression, improved focal adhesion turnover, and recovered the migratory capacity affected by HG/OC stress.

Discussion

Chronic HG stress did not decrease the ALDH2 activity or increase ROS in 3T3 fibroblasts

The inhibition of fibroblast cell migration by hyperglycemia is a well-known cause of diabetic complications[11,20–22]. Most studies provided mechanistical explanations related to a decreased ALDH2 activity, increased oxidative stress/senescence, and dysfunctional mitophagy[16,23–25]. However, in our model of ALDH2 overexpression, the 3T3 stable clones proliferated healthily after sub-cultured in HG/OC medium for 7 days, and flow cytometry revealed no elevation of cell death or oxidative stress. Even in cells with ALDH2 deficiency, where ROS did increase shortly after being exposed to disulfiram, the ROS was not significantly different between the C1 Ctrl + D vs. HG + D groups. The ALDH2 activities were indifferent between cells cultured in Ctrl/OC/HG medium. Even if these findings appeared contradicted with previous studies, we did demonstrate the significantly increased expression of paxillin, reorganization of ventral stress fibers to the trailing edge, and perinuclear mitochondrial clustering in the 3T3-C1 HG/OC subclones. This implies a possible different mechanism of HG-induced migratory inhibition in our model of chronic hyperglycemia.

Unlike previous studies, which often involved treatment protocols with a relatively short exposure (< 72 h) of cells to a wide range of D-glucose concentrations (5.5–75 mM)[21,22,26], fibroblasts in the present study were exposed to a relatively modest change in glucose concentration (+ 30 mM) for a longer period (7 days). We believe our design better mimics the pathogenesis of "chronic" diabetic complications, as cells are more likely to survive and change their protein expression to adapt for the HG stress[27,28]. Meanwhile, the ALDH2 activity assay used in our study was modified from methods published by Nannelli et al.[18], but we added all the cell lysate into the reaction buffer, rather than a portion with same amount of protein, because we assumed that fibroblasts adapted to chronic HG stress might increase their overall protein expression related to extracellular matrix and skewed the relative amount of ALDH2[28], so our method measured the exact change in ALDH2 activity per cell—as we seeded the same number of cells. Although these methodological differences account for some of the conflicting results, our research revealed that chronic HG/OC stress does not reduce ALDH2 activity or increase ROS in 3T3 fibroblasts, but it promotes cellular adaptation process associated with higher cellular adhesion.

Hyperglycemia might inhibit cell migration through mechanisms dependent on hyperosmolality and focal adhesion turnover

The present study demonstrated that prolonged exposure to HG medium induced a reorganization of stress fibers and enhanced expression of cell adhesion molecules in fibroblasts, making the cells less mobile and therefore difficult to migrate in the presence of spatial cues. To our knowledge, this is one of the few studies to illustrate a novel mechanism underlying HG-induced migratory inhibition by disrupting the efficient cytoskeleton remodeling and focal adhesions turnover[29,30]. In addition, the HG-induced migratory inhibition is dependent on hyperosmolar stress rather than on oxidative stress. An increasing number of studies have attributed the biological effects of hyperglycemia to the increase in osmolality[30–33], but very few of them have discussed its effects on cell migration. In a study using rat peritoneal mesothelial cells, high glucose/hyperosmolality inhibited cell migration through pathway involving the phosphorylation of focal adhesion kinase and its downstream p-130(Cas), an adaptor protein of actin filaments[30]. Researchers also found that when induced pluripotent stem cells were exposed to high glucose/mannitol medium, the formation of osmopodia (i.e. lamellipodia-like structures that are sensitive to osmolality) increased dramatically and started to anchor cells to the culture plate through actin polymerization[34]. Higher osmopodia formation frequency was associated with an increased expression of beta-catenin, a protein involved in the recruitment of cell adhesion molecules. Interestingly, in another study which concluded that elevated ROS was the cause of HG-induced migratory inhibition, the number of short-lived protrusions and RhoA activity were also increased in the OC group[35]. The RhoA/ROCK pathway facilitates the bundling of actin fibers and integrins into focal adhesions; when activated at the trailing edge, it is generally regarded as a promotor of strong adhesions and has a negative impact on cell migration[36]. In our study, both the expression of paxillin and disoriented actin filaments increased significantly in the 3T3-C1 HG/OC subclones. Considering the adaptive nature of 3T3 fibroblasts[37], we hypothesize that some cells developed higher adhesion strength to counteract the shrinkage/detachment induced by hyperosmolar stress.

HG-induced hyperosmolar stress triggered mitochondrial perinuclear clustering and impaired its interaction with focal adhesions

During migration, cells undergo rapid changes in shape at the migrating front. This is accomplished through reorganization of the cytoskeleton, which in turn requires mitochondrial energetics[7,38]. Actin filaments at the lamellipodia extend and retract, pushing the cell membrane forward. At the same time, mitochondria are dynamically transported along the cytoskeleton to regions of high-energy demand, such as the leading edge, under the support of various motor proteins[39–41]. Through mechanisms that involve mitochondrial Rho-GTPase 1 (Miro-1) motor protein, wound creation triggers the spatial redistribution of mitochondria, decreases focal adhesion stability, and promotes migratory behavior[42,43]. This highlights the interdependence of the cytoskeleton and mitochondria, and how their interactions are essential for cells to react to environmental cues[44–46]. In the current study, we found that mitochondrial networks underwent morphological changes to facilitate the

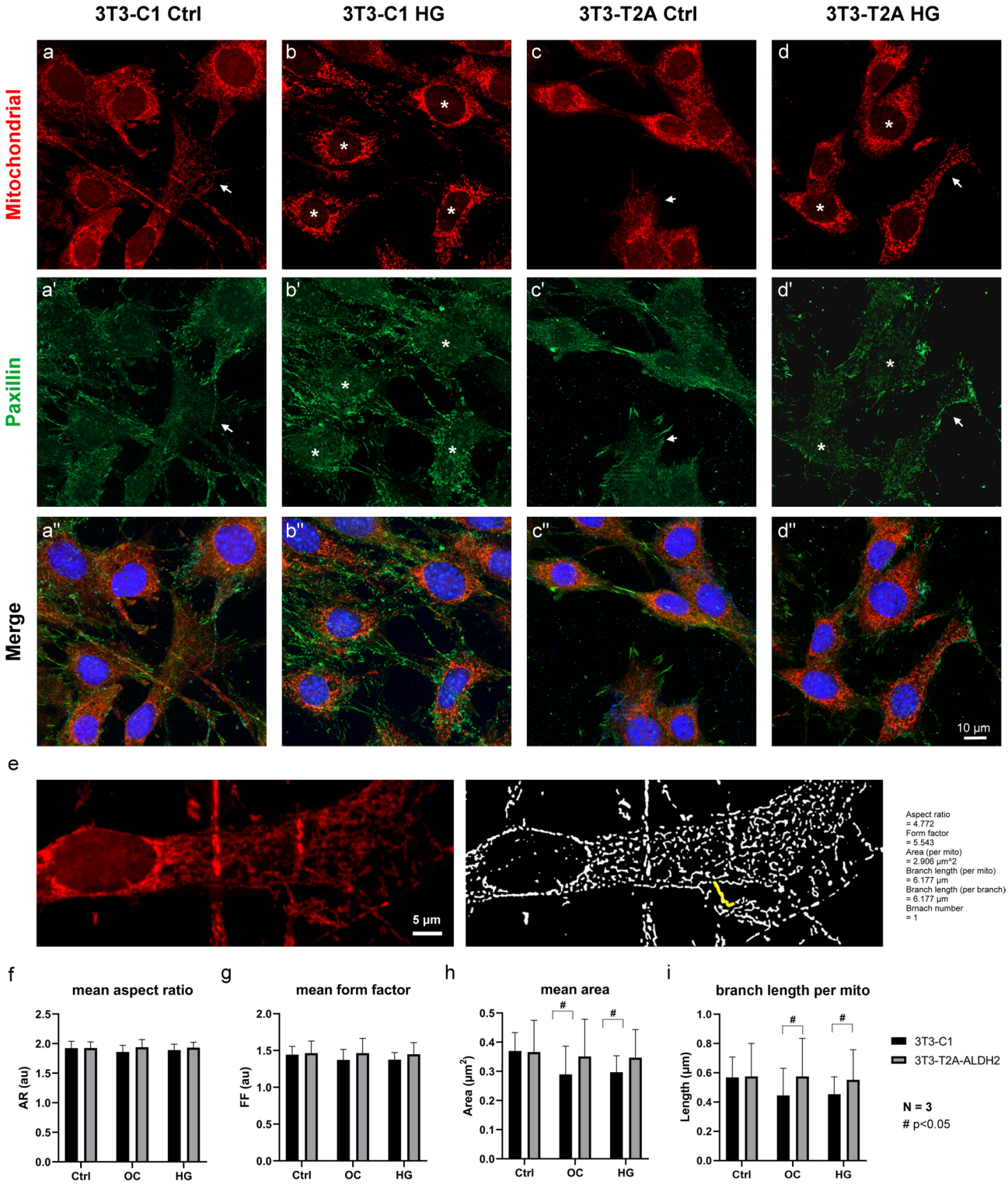

disassembly of focal adhesions. Without exposure to the HG/OC medium, the 3T3 fibroblasts had mostly nascent adhesion complex, and their mitochondrial networks often extended into the protruding lamellipodia. After adaptation to HG-induced hyperosmolar stress, however, the cells exhibited more disoriented stress fiber, more mature focal adhesions, and short/fragmented mitochondria that clustered perinuclearly. In fact, the spatial distributions of focal adhesions and mitochondria were almost completely separated, suggesting a lack of interactions in these non-migrating cells.

To the best of our knowledge, this is the first study to characterize the interactions between mitochondria and focal adhesions in cells chronically affected by HG-induced hyperosmolality. Researchers have long known that hyperglycemia can induce fission-like mitochondrial fragmentation, which increased the production of ROS and cell death[47,48]. This change in morphology occurs independently of protein O-GlcNAcylation[49], and it has been associated with decreases in mitochondrial ATP production and vesicle motility[50,51]. In the present

◀**Fig. 5**. The overexpression of ALDH2 preserved the elongated mitochondrial networks despite the presence of HG/OC stress. (**a**–**d**) In the 3T3-C1 Ctrl and 3T3-T2A Ctrl subclones, many cells had mitochondrial networks extending into their protruding lamellipodia (arrow), and their adhesion complex were mostly disassembled (**a'**, **c'**). On the contrary, in the 3T3-C1 HG subclone, most mitochondria clustered around their nuclei (asterisk), distant from those mature focal adhesions heavily stained with paxillin (**b'**). Both patterns of mitochondrial network could be found in the 3T3-T2A HG subclone, and there were only a few mature focal adhesions (**d'**). The merged images highlighted the spatial relationship between mitochondria and Paxillin (**a"**–**d"**). Scale bars = 10 μm. (**e**) Representative mitochondrial network from the 3T3-C1 Ctrl (arrow in **a**) and its skeletonization by the ImageJ tool Mitochondrial Analyzer. Parameters of the mitochondria colored yellow are listed on the right side. Scale bar = 5 μm. (**f**–**i**) Quantitative analysis of mitochondria revealed no difference in mean aspect ratio or form factors between different subclones. However, the mean area and branch length per mitochondria were significantly lower in the 3T3-C1 HG/OC subclones. The experiment was repeated independently 3 times, $p < 0.05$.

study, perinuclear mitochondrial networks were found predominantly in non-migrating cells with thick stress fibers and mature focal adhesions. Such a perinuclear staining pattern has also been found in mouse embryonic fibroblasts deficient of Miro-1 protein[42], and it has been shown to dramatically decrease adenosine triphosphate (ATP) production at the cell periphery, disrupting energy-dependent events such as lamellipodia protrusion[43]. The mitochondrial fragmentation indicates a possible osmoregulation process essential to maintain cristae architecture and more efficient ATP sythesis[52].

ALDH2 overexpression ameliorated the HG-induced migratory inhibition by enhancing mitochondrial elongation and focal adhesion turnover

The initial goal of this study was to determine how ALDH2 affects the behavior of cells under chronic hyperglycemia conditions. Several studies have reported the deleterious effect of ALDH2 inhibition on cell survival and proliferation, either with or without hyperglycemic stress[18,53]. The overexpression of ALDH2 on cardiomyocytes has been shown to alleviate HG-induced cell death[54]. In addition, a previous study reported significantly increased apoptosis in cardiac fibroblasts exposed to HG medium, and that this effect could be rescued by an ALDH2 agonist[55]. Nevertheless, no studies have described how ALDH2 affects cell migration inhibited by chronic hyperglycemia. Our results revealed that the suppression of ALDH2 by disulfiram could not only trigger cell death and amplify oxidative stress, but it also enhanced the migratory inhibition caused by HG/OC medium. Conversely, the overexpression of ALDH2 could counteract this HG-induced migratory inhibition, as the 3T3-ALDH2 HG/OC subclones all had smaller residual gaps in the wound healing assay. Since fibroblasts often have a relatively high basal expression of ALDH2[55], we hypothesize that ALDH2 plays a crucial role in how fibroblasts adapt to chronic hyperglycemia. Disruption of this protective mechanism leads to failure of the cells to adapt and enter the cell death/apoptosis process. The overexpression of ALDH2 enhanced this protective effect and caused the cells to become more resistant to the migratory inhibition induced by hyperglycemia.

How exactly ALDH2, a redox enzyme located in the mitochondrial matrix, becomes involved in the cellular protective mechanism against chronic hyperglycemia is still under investigation. Most researchers agree that ALDH2 is crucial for maintaining mitochondrial homeostasis, a process commonly impaired during the pathogenesis of various diseases[56–58]. In a myocardial ischemic/reperfusion-induced myocardial injury model, ALDH2 was shown to preserve mitochondrial morphology and reduce cardiomyocyte apoptosis by inhibiting mitochondrial fission[57]. Furthermore, in acute kidney injury, ALDH2 has been shown to not only decrease the quantity of swollen mitochondria and ruptured cristae, but also to promote the nuclear translocation of PGC-1α, a key regulator of mitochondrial biogenesis[58]. In the present study, the overexpression of ALDH2 restored the ability to form larger mitochondrial network with longer branch length in the 3T3-T2A HG/OC subclones. Under conditions of HG-induced hyperosmolality, which tends to cause mitochondria to become swollen and fragmented, ALDH2 helps to maintain the networks extending to the cell periphery. This further allows for interactions between mitochondria and the cytoskeleton at the leading edge, restoring the efficient turnover of focal adhesions.

Conclusions

In summary, we found that chronic hyperglycemia could inhibit cell migration without increasing oxidative stress in the 3T3 fibroblasts. The underlying mechanism involved an increase in cell adhesion and mitochondrial perinuclear clustering, which prohibits the generation of ATP at the leading edge, a process crucial for the efficient turnover of focal adhesions. ALDH2 inhibition aggravated this process, and the overexpression of ALDH2 restored the migratory ability inhibited by HG-induced hyperosmolality. We demonstrated that ALDH2 overexpression preserves the ability of mitochondrial network to extend to the migrating fronts despite the presence of hyperglycemic stress. The overexpression of ALDH2 also prevented the formation of mature focal adhesions and disoriented stress fibers, suggesting an enhancement of focal adhesion turnover. The major limitation of this study is that we did not directly visualize the dynamic interactions between mitochondria and focal adhesions. However, no studies have reported similar findings, and we are the first to establish stable clones of fibroblasts overexpressing ALDH2, which prevents off-target effects of agonists and makes comparisons after HG adaptation possible. Future studies are needed to confirm our findings and investigate whether they also apply to other cell types.

Data availability

All data generated or analyzed during this study are included in this published article (and its Supplementary Information files).

Received: 15 July 2024; Accepted: 8 May 2025
Published online: 22 May 2025

References

1. Emily Joo, E. & Yamada, K. M. Cell adhesion and movement. In *Stem Cell Biology and Tissue Engineering in Dental Sciences* 61–72 (Elsevier, 2015). https://doi.org/10.1016/B978-0-12-397157-9.00005-9.
2. Carmeliet, P. & Jain, R. K. Molecular mechanisms and clinical applications of angiogenesis. *Nature* **473**, 298–307 (2011).
3. Hohmann, T. & Dehghani, F. The cytoskeleton—A complex interacting meshwork. *Cells* **8**, 1–55 (2019).
4. Dogterom, M. & Koenderink, G. H. Actin–microtubule crosstalk in cell biology. *Nat. Rev. Mol. Cell Biol.* **20**, 38–54 (2019).
5. Zaidel-Bar, R., Milo, R., Kam, Z. & Geiger, B. A paxillin tyrosine phosphorylation switch regulates the assembly and form of cell-matrix adhesions. *J. Cell. Sci.* **120**, 137–148 (2007).
6. Rajah, A. et al. Paxillin S273 phosphorylation regulates adhesion dynamics and cell migration through a common protein complex with PAK1 and βPIX. *Sci. Rep.* **9**, 11430 (2019).
7. Nagano, M., Hoshino, D., Koshikawa, N., Akizawa, T. & Seiki, M. Turnover of focal adhesions and cancer cell migration. *Int. J. Cell Biol.* https://doi.org/10.1155/2012/310616 (2012).
8. Lv, Z. et al. Fyn mediates high glucose-induced actin cytoskeleton reorganization of podocytes via promoting ROCK activation in vitro. *J. Diabetes Res.* **2016**, 1–13 (2016).
9. Lamers, M. L., Almeida, M. E. S., Vicente-Manzanares, M., Horwitz, A. F. & Santos, M. F. High glucose-mediated oxidative stress impairs cell migration. *PLoS ONE* **6**, 1–9 (2011).
10. Kemeny, S. F., Cicalese, S., Figueroa, D. S. & Clyne, A. M. Glycated collagen and altered glucose increase endothelial cell adhesion strength. *J. Cell. Physiol.* **228**, 1727–1736 (2013).
11. Burgess, J. L., Wyant, W. A., Abujamra, B. A., Kirsner, R. S. & Jozic, I. Diabetic wound-healing science. *Medicina (Lithuania)* **57**, 1072. https://doi.org/10.3390/medicina57101072 (2021).
12. Strickland, K. C., Holmes, R. S., Oleinik, N. V., Krupenko, N. I. & Krupenko, S. A. Phylogeny and evolution of aldehyde dehydrogenase-homologous folate enzymes. *Chem. Biol. Interact.* **191**, 122–128 (2011).
13. Lin, C. L. et al. The aldehyde dehydrogenase aldh2*2 allele, associated with alcohol drinking behavior, dates back to prehistoric times. *Biomolecules* **11**, 1376 (2021).
14. Steinmetz, C. G., Xie, P., Weiner, H. & Hurley, T. D. Structure of mitochondrial aldehyde dehydrogenase: The genetic component of ethanol aversion. *Structure* **5**, 701–711 (1997).
15. Chang, Y. C. et al. A common East-Asian ALDH2 mutation causes metabolic disorders and the therapeutic effect of ALDH2 activators. *Nat. Commun.* **14**, 5971 (2023).
16. Liu, X. W. et al. Deficiency of mitochondrial aldehyde dehydrogenase increases type 2 diabetes risk in males via autophagy dysregulation. *Chin. Med. J.* **134**, 2246–2248. https://doi.org/10.1097/CM9.0000000000001408 (2021).
17. Li, Y. C., Chen, S. J. & Chien, C. L. Erythropoietin produced by genetic-modified NIH/3T3 fibroblasts enhances the survival of degenerating neurons. *Brain Behav.* **5**, e00356. https://doi.org/10.1002/brb3.356 (2015).
18. Nannelli, G. et al. ALDH2 activity reduces mitochondrial oxygen reserve capacity in endothelial cells and induces senescence properties. *Oxid. Med. Cell. Longev.* **2018**, 9765027. https://doi.org/10.1155/2018/9765027 (2018).
19. Chaudhry, A., Shi, R. & Luciani, D. S. A pipeline for multidimensional confocal analysis of mitochondrial morphology, function, and dynamics in pancreatic-cells. *Am. J. Physiol. Endocrinol. Metab.* **318**, 87–101 (2020).
20. Lerman, O. Z. et al. Cellular dysfunction in the diabetic fibroblast impairment in migration, vascular endothelial growth factor production, and response to hypoxia. *Am. J. Pathol.* **162**, 303 (2003).
21. Buranasin, P. et al. High glucose-induced oxidative stress impairs proliferation and migration of human gingival fibroblasts. *PLoS ONE* **13**, 1–19 (2018).
22. Xuan, Y. H. et al. High-glucose inhibits human fibroblast cell migration in wound healing via repression of bFGF-regulating JNK phosphorylation. *PLoS One* **9**, e108182 (2014).
23. Gao, J., Hao, Y., Piao, X. & Gu, X. Aldehyde dehydrogenase 2 as a therapeutic target in oxidative stress-related diseases: Post-translational modifications deserve more attention. *Int. J. Mol. Sci.* **23**, 2682. https://doi.org/10.3390/ijms23052682 (2022).
24. Wei, Y. et al. Aldehyde dehydrogenase 2 deficiency aggravates lung fibrosis through mitochondrial dysfunction and aging in fibroblasts. *Am. J. Pathol.* **194**, 1458–1477 (2024).
25. Nannelli, G., Ziche, M., Donnini, S. & Morbidelli, L. Endothelial aldehyde dehydrogenase 2 as a target to maintain vascularwellness and function in ageing. *Biomedicines* **8**, 1–12 (2020).
26. Soydaş, T. et al. Effects of short-term high glucose on NIH/3T3 fibroblast proliferation, apoptosis, and collagen type I production. *Tıp Fakültesi Klinikleri Dergisi* **2**, 91–95 (2019).
27. Cheng, Y. et al. Central role of cardiac fibroblasts in myocardial fibrosis of diabetic cardiomyopathy. *Front. Endocrinol.* **14**, 1162754. https://doi.org/10.3389/fendo.2023.1162754 (2023).
28. Tuleta, I. & Frangogiannis, N. G. Fibrosis of the diabetic heart: Clinical significance, molecular mechanisms, and therapeutic opportunities. *Adv. Drug Deliv. Rev.* **176**, 113904 (2021).
29. Lv, Z. et al. Fyn mediates high glucose-induced actin cytoskeleton reorganization of podocytes via promoting ROCK activation in vitro. *J. Diabetes Res.* **2016**, 1–13 (2016).
30. Tamura, M. et al. High glucose levels inhibit focal adhesion kinase-mediated wound healing of rat peritoneal mesothelial cells. *Kidney Int.* **63**, 722 (2003).
31. Madonna, R. et al. Simulated hyperglycemia impairs insulin signaling in endothelial cells through a hyperosmolar mechanism. *Vascul. Pharmacol.* **130**, 106678 (2020).
32. Mussi, N., Stuard, W. L., Sanches, J. M. & Robertson, D. M. Chronic hyperglycemia compromises mitochondrial function in corneal epithelial cells: Implications for the diabetic cornea. *Cells* **11**, 2567 (2022).
33. Kambayashi, R. et al. Both osmolality-dependent and independent mechanisms are associated with acute hyperglycemia-induced cardiovascular adverse reactions: Analysis of the mutual interactions leading to cardiovascular phenotypes in dogs. *J. Toxicol. Sci.* **48**, 169–178 (2023).
34. Madonna, R., Geng, Y. J., Shelat, H., Ferdinandy, P. & De Caterina, R. High glucose-induced hyperosmolarity impacts proliferation, cytoskeleton remodeling and migration of human induced pluripotent stem cells via aquaporin-1. *Biochim. Biophys. Acta Mol. Basis Dis.* **1842**, 2266–2275 (2014).
35. Lamers, M. L., Almeida, M. E. S., Vicente-Manzanares, M., Horwitz, A. F. & Santos, M. F. High glucose-mediated oxidative stress impairs cell migration. *PLoS ONE* **6**, 1–9 (2011).
36. O'Connor, K. L. & Chen, M. Dynamic functions of RhoA in tumor cell migration and invasion. *Small GTPases* **4**, 141 (2013).
37. Rubin, H. & Xu, K. Evidence for the progressive and adaptive nature of spontaneous transformation in the NIH 3T3 cell line. *Proc. Natl. Acad. Sci.* **86**, 1860 (1989).

38. Madan, S., Uttekar, B., Chowdhary, S. & Rikhy, R. Mitochondria lead the way: Mitochondrial dynamics and function in cellular movements in development and disease. *Front. Cell. Dev. Biol.* **9**, 1–23 (2022).
39. Pilling, A. D., Horiuchi, D., Lively, C. M. & Saxton, W. M. Kinesin-1 and dynein are the primary motors for fast transport of mitochondria in *Drosophila* motor axons. *Mol. Biol. Cell.* **17**, 2057–2068 (2006).
40. Zhao, J. et al. Mitochondrial dynamics regulates migration and invasion of breast cancer cells. *Oncogene* **32**, 4814–4824 (2013).
41. Cunniff, B., McKenzie, A. J., Heintz, N. H. & Howe, A. K. AMPK activity regulates trafficking of Mitochondria to the leading edge during cell migration and matrix invasion. *Mol. Biol. Cell.* **27**, 2662–2674 (2016).
42. Fu, H. et al. Wounding triggers MIRO-1 dependent mitochondrial fragmentation that accelerates epidermal wound closure through oxidative signaling. *Nat. Commun.* **11**, 1050 (2020).
43. Schuler, M. H. et al. Miro1-mediated mitochondrial positioning shapes intracellular energy gradients required for cell migration. *Mol. Biol. Cell.* **28**, 2159–2169 (2017).
44. Otera, H. & Mihara, K. Mitochondrial dynamics: Functional link with apoptosis. *Int. J. Cell. Biol.* **2012**, 1–10 (2012).
45. Galloway, C. A. & Yoon, Y. Mitochondrial morphology in metabolic diseases. *Antioxid. Redox Signal.* **19**, 415–430 (2013).
46. Zhou, W. et al. Mitofusin 2 regulates neutrophil adhesive migration and the actin cytoskeleton. *J. Cell Sci.* **133**, jcs248880 (2021).
47. Yu, T., Sheu, S. S., Robotham, J. L. & Yoon, Y. Mitochondrial fission mediates high glucose-induced cell death through elevated production of reactive oxygen species. *Cardiovasc. Res.* **79**, 341–351 (2008).
48. Roy, S., Kim, D. & Sankaramoorthy, A. Mitochondrial structural changes in the pathogenesis of diabetic retinopathy. *J. Clin. Med.* **8**(9), 1363 (2019).
49. Dassanayaka, S. et al. High glucose induces mitochondrial dysfunction independently of protein O-GlcNAcylation. *Biochem. J.* **467**, 115–126 (2015).
50. Moruzzi, N. et al. Short and prolonged exposure to hyperglycaemia in human fibroblasts and endothelial cells: Metabolic and osmotic effects. *Int. J. Biochem. Cell Biol.* **53**, 66–76 (2014).
51. Nunes, P. et al. Ionic imbalance, in addition to molecular crowding, abates cytoskeletal dynamics and vesicle motility during hypertonic stress. *Proc. Natl. Acad. Sci. U. S. A.* **112**, E3104–E3113 (2015).
52. Austin, S. & Nowikovsky, K. Mitochondrial osmoregulation in evolution, cation transport and metabolism. *Biochim. Biophys. Acta Bioenerg.* **1862**, 148368 (2021).
53. Pan, G., Deshpande, M., Thandavarayan, R. A. & Palaniyandi, S. S. ALDH2 inhibition potentiates high glucose stress-induced injury in cultured cardiomyocytes. *J. Diabetes Res.* https://doi.org/10.1155/2016/1390861 (2016).
54. Cao, R. et al. ALDH2 overexpression alleviates high glucose-induced cardiotoxicity by inhibiting NLRP3 inflammasome activation. *J. Diabetes Res.* **2019**, 4857921 (2019).
55. Gu, X. et al. Effect of ALDH2 on high glucose-induced cardiac fibroblast oxidative stress, apoptosis, and fibrosis. *Oxid. Med. Cell Longev.* **2017**, 9257967 (2017).
56. Ji, W. et al. Aldehyde dehydrogenase 2 protects against lipopolysaccharide-induced myocardial injury by suppressing mitophagy. *Front. Pharmacol.* **12**, 641058 (2021).
57. Zhang, R. Aldehyde dehydrogenase 2 preserves mitochondrial morphology and attenuates hypoxia/reoxygenation-induced cardiomyocyte injury. *World J. Emerg. Med.* **11**, 246 (2020).
58. Li, J. et al. Aldehyde dehydrogenase 2 alleviates mitochondrial dysfunction by promoting PGC-1α-mediated biogenesis in acute kidney injury. *Cell Death Dis.* https://doi.org/10.1038/s41419-023-05557-x (2023).

Acknowledgements

We thank research assistant Mei-Hsiang Hsu for her valuable efforts in the conduction of experiments and collection of data. This study was supported by research grants 106-FEMH-FJU-05, 107-FEMH-FJU-03 (CC.H.) from Far Eastern Memorial Hospital and Fu Jen Catholic University Joint Research Program, MOST 110-2314-B-418-011-MY2 (CC.H.), and NSTC 112-2320-B-002-036 (CL.C) from the Ministry of Science and Technology of Taiwan. The funders had no role in study design, data collection and analysis, decision to publish, or preparation of the manuscript.

Author contributions

Chi-Cheng Huang analyzed the data and wrote the main manuscript text. Chung-Liang Chien helped to design the study, and Yuh-Lien Chen helped to interpretate the data.

Declarations

Competing interests

The authors report no relationships that could be construed as a conflict of interest.

Additional information

Supplementary Information The online version contains supplementary material available at https://doi.org/10.1038/s41598-025-02022-x.

Correspondence and requests for materials should be addressed to C.-L.C.